ADVANCED FUNCTIONAL MATERIALS
www.afm-journal.de

www.MaterialsViews.com

Interaction of Carbon Coating on $LiFePO_4$: A Local Visualization Study of the Influence of Impurity Phases

*Jiajun Wang, Jinli Yang, Yong Zhang, Yongliang Li, Yongji Tang, Mohammad Norouzi Banis, Xifei Li, Guoxian Liang, Ruying Li, and Xueliang Sun**

Carbon coating is a proven successful approach for improving the conductivity of $LiFePO_4$ used in rechargeable Li-ion batteries. Different impurity phases can be formed during $LiFePO_4$ synthesis. Here, a direct visualization of the impact of impurity phases in $LiFePO_4$ on a carbon coating is presented; they are investigated on a model material using various surface-characterization techniques. By using polished ingot model materials, impurity phases can be clearly observed, identified, and located on the surface of the sample by scanning electron microscopy (SEM), focused-ion-beam lithography (FIB), high-resolution transmission electron microscopy (HR-TEM), and Raman spectroscopy. During the carbon-coating process, the phosphorus-rich phase is found to have an inhibiting effect (or no positive catalytic effect) on carbon formation, while iron-rich phases (mainly iron phosphides) promote carbon growth by contributing to more carbon deposition and a higher graphitic carbon content. This finding, and the methodological evaluation here, will help us to understand and reveal the influencing factors of impurity phases on the basic carbon-deposition process to obtain high-performance $LiFePO_4$ material for future energy-storage devices.

1. Introduction

As a well-known positive material for lithium-ion batteries, phospho-olivine $LiFePO_4$ has attracted increasing attention from both the academic and the industrial community. Indeed, this material has a high theoretical capacity of 170 mA h g^{-1} and can offer many inherent advantages such as safety, environmental benignity, and low toxicity.[1] The main drawback of this material is its intrinsic poor electrical conductivity, which can be overcome by using a thin layer of carbon coating on nano-sized $LiFePO_4$, and has been successfully commercialized.[2]

Since carbon coating was first introduced to improve the conductivity of $LiFePO_4$, extensive research has been performed on its impact on the physical and electrochemical performance of $LiFePO_4$.[3–9] These details of carbon coating include: i) carbon content and carbon thickness: an appropriate carbon content with a thin carbon coating is critical considering the balance of sufficient conductivity and easy lithium-ion penetration;[4] ii) carbon nature: graphitic carbon is more desirable due to its excellent electronic conductivity;[5,6] iii) carbon morphology and distribution: a uniform and full carbon coating can ensure $LiFePO_4$ particles get electrons from all directions and alleviates the polarization phenomenon;[7] iv) carbon surface and porosity: a porous carbon film with a high surface area enhances the electronic contact between the grains, contributing to a higher conductivity;[8] v) carbon precursors: in situ decomposition or pyrolysis of organic carbon sources result in a more-uniform graphitic carbon film on the surface of $LiFePO_4$.[9] In addition to the direct contribution to conductivity as discussed above, carbon coating may also bring some conductive metal phosphides during the synthesis process of $LiFePO_4$,[10,11] which contributes to the increased electronic conductivity of $LiFePO_4$.

While numerous studies have been devoted to seeking better carbon coatings for $LiFePO_4$, detailed studies on the effect of the $LiFePO_4$ surface and impurity phases on carbon coating are scarce. It is well known that it is hard to avoid some impurity phases during the synthesis process, such as the solid-state method, where an inhomogeneous mixture occurs and trivalent ions have extremely low diffusion coefficients in the solid-state, resulting in parallel reactions and inhomogeities.[12] For example, some impurities (e.g., Fe_2P, $Li_4P_2O_7$, and Li_3PO_4) often form together with the olivine $LiFePO_4$ and have been widely detected in numerous studies.[12–16] In addition, to reduce the materials and preparation cost, natural triphylite mineral is a good choice for industrial production and applications of $LiFePO_4$, but this natural material will also bring more impurity phases.[2,12] Some impurity phases may exist in naturally occurred triphylite mineral in the form of $Fe_3(PO_4)_2(OH)_2$, $Fe_3(PO_4)_2$, and other phases.[12] The presence of these inactive impurities may not only decrease utilization of $LiFePO_4$, but also significantly affect the physical and electrochemical properties of $LiFePO_4$. For example, an appropriate amount of Fe_2P

Dr. J. Wang, J. Yang, Dr. Y. Zhang, Y. Li, Dr. Y. Tang, M. N. Banis, Dr. X. Li, R. Li, Prof. X. Sun
Department of Mechanical and Materials Engineering
University of Western Ontario
London, Ontario, N6A 5B9 Canada
E-mail: xsun@eng.uwo.ca
Dr. G. Liang
Phostech Lithium Inc, 1475 Rue Marie-Victorin
St-Bruno, QC, J3V 6B7 Canada

DOI: 10.1002/adfm.201201310

increases $LiFePO_4$ conductivity, while excess amounts may block the lithium-ion paths.[17] Therefore, a study of impurities is necessary for the development of $LiFePO_4$. For the same reason, the research on whether these impurity phases can affect the carbon coating is also critical for C/$LiFePO_4$. Unfortunately, so far, few investigations have been performed on it. The main reason is the lack of appropriate model materials for such a study. Most researchers have worked on micro- and nanosized $LiFePO_4$, which is difficult to clearly observe and identify the impurity phases on $LiFePO_4$.

Our aim of this present work is to clarify whether there is an effect of impurity phases on carbon coating for $LiFePO_4$ and how they affect carbon coating in comparison with carbon deposition from the gas phase on a pristine $LiFePO_4$ pure phase, which is also known to catalyze carbon deposition and form a thin nanocoating of carbon. In this paper, our investigations were performed on ingot samples with a flat surface. This model material allows us to identify and observe some impurity phases clearly on the surface of $LiFePO_4$. The structural and morphological information were determined from micro X-ray diffraction (μXRD), high-resolution scanning electron microscopy (SEM), focused-ion-beam, high-resolution transmission electron microscopy (HR-TEM), and micro Raman spectroscopy measurements. By combining these material-characterization techniques, it allows us to intensively investigate and identify the nature and effects of impurity phases on carbon coating for $LiFePO_4$. In this study, for the first time, the P-rich phase are found to have a slightly inhibiting effect (or no positive catalytic effect) on carbon coating, while Fe-rich phases (mainly iron phosphides) promote carbon coating by contributing to more carbon deposition and a higher content of graphitic carbon. Our report provides direct proof about the effects of these typical impurity phases on the morphology and structure of a carbon coating on $LiFePO_4$.

2. Results and Discussion

Impurity phases often form together with olivine $LiFePO_4$. In order to identify the possible impurity phases in $LiFePO_4$ ingots, the X-ray diffraction pattern was collected for the ingot samples and the resultant XRD pattern is shown in **Figure 1**a. The ingot material is mainly $LiFePO_4$, which contains a small amount of impurity phases. These minor impurity phases in the general Li-Fe^{3+}/Fe^{2+}-P-O system include $Li_4P_2O_7$ (P-rich phases) and Fe_2P (Fe-rich phases), and other impurity phases with trace amounts. Many of these impurity phases are also detected by other studies using various synthesis methods,[12–16] and detailed characterization of these impurities in this ingot sample has been reported in our previous work.[12]

In order to observe and detect the impurity phases on the surface of the ingot sample, energy dispersive X-ray (EDX) element mapping was performed in field-emission SEM (FE-SEM). Figure S1 in the Supporting Information shows direct evidence of the existence of two typical phases on the ingot surface. By using the back-scattering technique under a high accelerated voltage in FE-SEM, obvious different phases with a darker color were found to be distributed in the regions near to the grain boundaries, as marked with a dashed rectangle (Supporting Information, Figure S1a). The element mapping (Figure 1b) shows that this dark zone consists of an impurity phase with an Fe-deficient and P-rich (low Fe/P ratio) composition, while oxygen was found to be homogeneously distributed on the entire surface, so we called it the P-rich phase. To determine the ratio of the elements on this surface, EDX analysis was performed and the dark zone shows 6:26:68 for the relative atomic ratio of Fe, P, and O (EDX not shown here). It should be noted that EDX does not show lithium due to its low electron-scattering cross section.

Figure S1b in the Supporting Information shows another typical impurity phase observed on the sample. These phases were also observed to be mainly located at local defects or porosities around the grain boundaries on the ingot sample, where lithium could be lost and the crystal surface is reduced to iron phosphides. From the element mapping (Figure 1c), it can be clearly seen that both oxygen and phosphorus are deficient in this phase; thus, we call it an Fe-rich phase. EDX analysis further indicates that the relative atomic ratio of Fe, P, and O is 54:16:30 (EDX not shown here). All of the above observations confirm the existence of the typical impurity phases on the surface of the ingot samples. The formation of these impurity phases is associated with the solidification process. During the cooling process, $LiFePO_4$ crystallizes, and excess non-stoichiometric reactants are rejected from the growth of $LiFePO_4$ crystals during progressive solidification, thus making these impurities separate from $LiFePO_4$ and locate at the boundaries. This makes the metallurgical method a promising one for the synthesis of highly pure $LiFePO_4$ and, meanwhile, allows us to find easily and observe clearly the impurity phases.

The carbon coating was carried out using the spray pyrolysis chemical vapor deposition (CVD) process.[18–20] The advantage of this method is the well-controlled carbon-coating process on $LiFePO_4$ (including the carbon content, carbon thickness, deposition temperature, and time) on the surface of ingot sample. From the SEM images (Supporting Information, Figure S2), a brighter color was found on the carbon-coated sample, indicating the conductive carbon-layer coating on the sample. In particular, a clearer carbon layer was easily found at the boundaries, further suggesting the successful carbon coating on the ingot sample. Here, we focus on the impact of surface impurity phases on carbon coating, as shown in **Figure 2**. Figure 2a,b show the surface morphologies of a typical area on the ingot sample before and after carbon coating. This area contains $LiFePO_4$ and both of the above-mentioned impurity phases. From the SEM images, no obvious morphology changes are found on the carbon-coated sample, but the color becomes brighter, which is due to the presence of the highly conductive carbon film covering the surface. Here, the P-rich phase can be seen clearly at the dark zone (marked with dashed square frame) in Figure 2b. EDX analysis indicated the relative atomic ratio among P, Fe, O, and C is 16:2:77:5 (Figure 2d). Here, the carbon fraction is lower than that of bulk, where it shows a relative atomic ratio of 9:8:70:13 (Figure 2c), indicating that the P-rich phase has an inhibiting effect (or no catalytic effect) on carbon deposition, as compared with $LiFePO_4$ or Fe-P-rich phases. Indeed, it was found that the addition of phosphorus in the carbon precursor has an inhibiting effect on the deposition and growth of various carbon materials, such as carbon

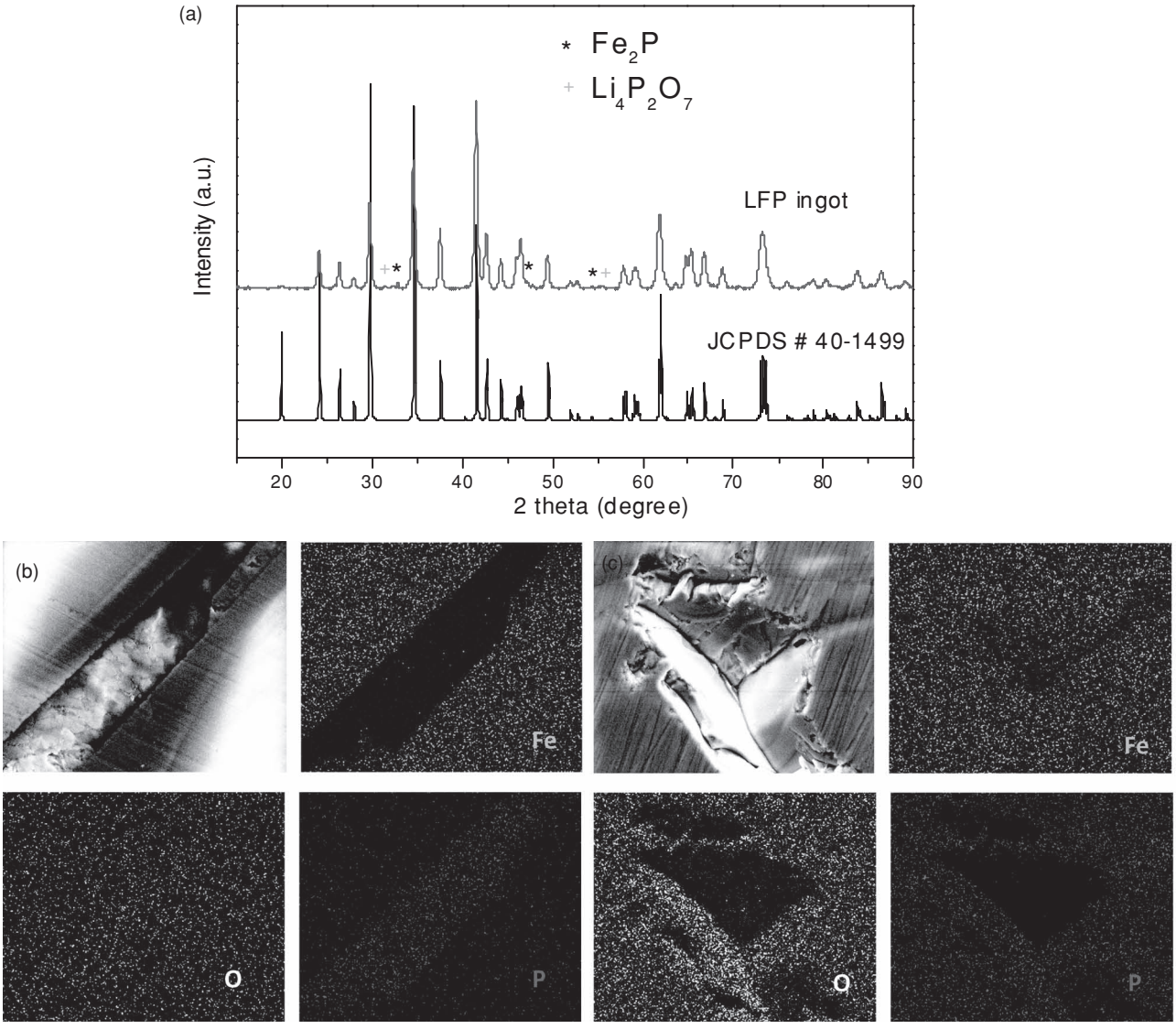

Figure 1. a) XRD pattern of the impurities in $LiFePO_4$ ingot sample. b) SEM element mappings of P-rich, Fe-deficient phases (called P-rich phases). c) SEM element mappings of P-O-deficient phases (called Fe-rich phases) on $LiFePO_4$.

nanofibers and carbon nanotubes.[21,22] In contrast, iron phosphide (or Fe-P-rich) zones show a carbon content significantly higher than the bulk. As shown by EDX, the relative atomic ratio between P, Fe, O, and C in this phase is 7:21:37:35, where the carbon composition is more than twice that of the bulk (Figure 2e). The reason can be attributed to the presence of these Fe-rich phases because these phases are known as a catalyst for the synthesis of various carbon materials such as carbon nanotubes.[23]

In order to further verify the role of Fe-rich phases on carbon coating, focused-ion-beam lithography (FIB) and HR-TEM were used to study the cross section consisting of the carbon coating, $LiFePO_4$, and the interface. Firstly, a small piece of a typical sample was prepared using the focused-ion-beam technique. **Figure 3**a shows the slicing and plucking process. A slice of the sample with thickness of ≈50 nm was thus obtained for HR-TEM analysis. The selected zone was located at the cracks of the sample, where many Fe-rich phases usually exist. Figure 3b shows a low-magnification TEM image of the sliced sample. It was found that these impurities were distributed non-uniformly and showed irregular shapes (green arrows and the green circle in the inset in Figure 3b). The following HR-TEM images in Figure 3c,d clearly show the role of impurities on carbon coating. Carbon with a thickness of ≈10 nm was coated on the bulk $LiFePO_4$ material, while more than 30 nm of carbon was found on the Fe-rich impurity phase due to its high catalytic effect. In comparison, a carbon layer of less than 5 nm was coated on the P-rich phase due to the inhibiting effect (or no positive catalytic effect) of phosphorus on the carbon coating (Supporting Information, Figure S3). Selected area electron diffraction (SAED) measurements indicated these impurities correspond to the Fe-rich phase of Fe_2P, and the bulk is $LiFePO_4$. EDX results further confirmed that the impurity phase has a higher Fe/P ratio than bulk $LiFePO_4$. Furthermore, EDX also

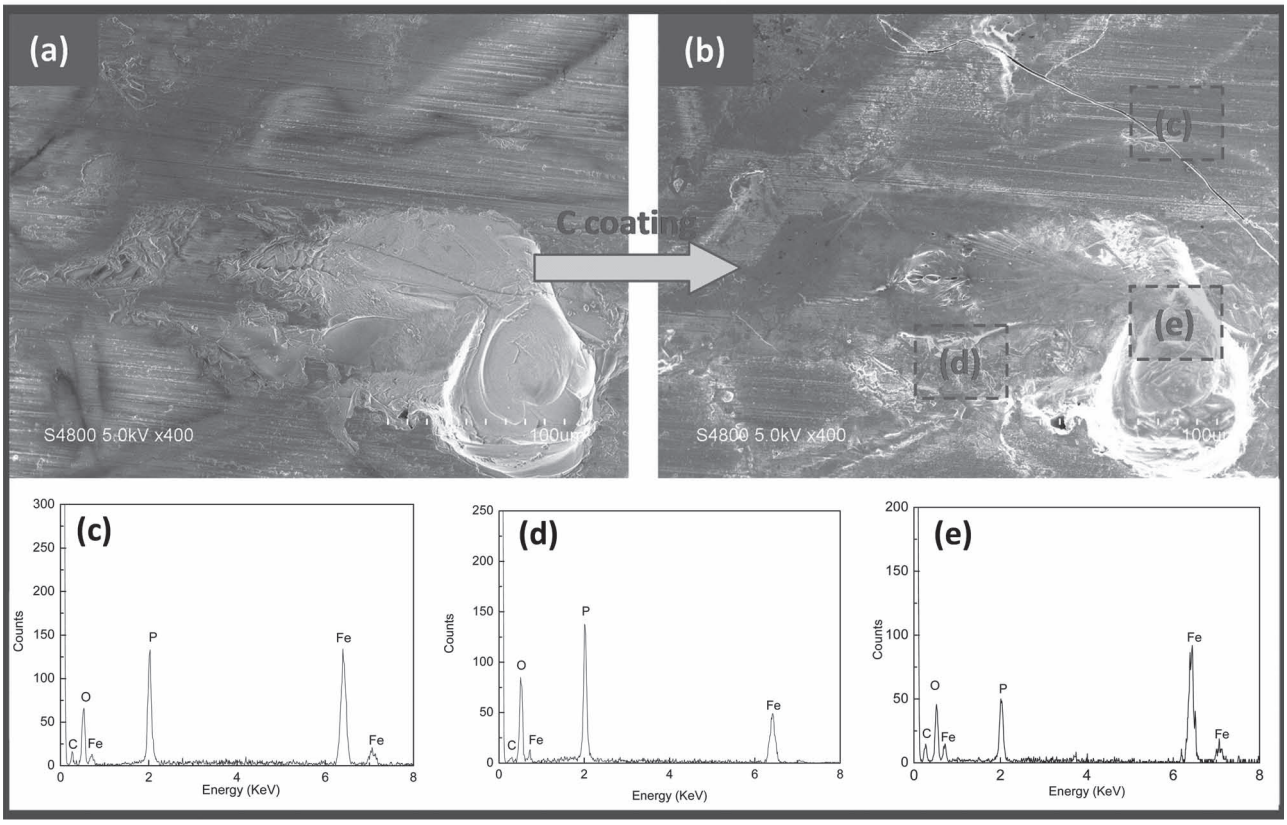

Figure 2. SEM-EDX analysis of carbon coated on impurity phases of $LiFePO_4$. a) Image of impurities before carbon coating. b) Image of impurities after carbon coating (the bulk, P-rich, and Fe-rich phases are marked as c, d, and e, respectively). c) EDX of carbon coating on the bulk phase. d) EDX of carbon coating on the P-rich phase. e) EDX of carbon coating on the Fe-rich phase.

showed a higher concentration of carbon existing on this Fe-rich phase than the bulk, which further confirms that the Fe-rich phase has a promoting effect of carbon deposition.

In addition to the contribution to the higher carbon content, the Fe-rich (mainly Fe_2P) phases were found to have an important influence on the structure of the formed carbon coating. The evidence could be obtained from Raman spectroscopy. Figure S4 in the Supporting Information shows the Raman spectra for two typical zones (bulk and gap) of the carbon-coated ingot sample. The gap zone was generally associated with Fe-rich phases, as discussed above. We observed intense Raman spectroscopy modes at 216, 278, 390, 441, 950, 992, and 1045 cm^{-1}, and comparatively less-intense Raman spectroscopy modes at 429, 560, and 626 cm^{-1} in pristine C-$LiFePO_4$, which is comparable with previously reported Raman spectra of C-$LiFePO_4$ with the same orthorhombic symmetry.[24–26] Two intense broad bands at 1350 and 1585 cm^{-1} could be assigned to the D and G bands of coated carbon on the surface of a $LiFePO_4$ ingot sample, respectively.[27] The D mode is generally associated with defects in the graphene sheet and staging disorder, while the G mode is a characteristic feature of graphitic layers. The peak intensity ratio of I_G/I_D can be recognized as the index of the degree of ordering, and a higher value of the ratio reflects a greater graphitic degree. The calculated results were 1.05 and 1.25 for the bulk and gap zones, respectively, indicating that the carbon precursor was decomposed to form a more highly graphitized carbon at the Fe-rich zone.

It is well known that iron has a positive effect on the decomposition/deposition of carbon precursors and is an ideal catalyst for the growth of high-quality carbon materials such as carbon nanotubes.[28,29] The catalytic roles come from two main reasons. One is the decrease of the pyrolysis temperature of the carbon precursor with iron catalysis. Therefore the carbon deposition rate increases and more carbon can be coated on the Fe-rich phases (the Fe_2P impurities in this work).[30,31] The other reason is related to iron atom diffusion and carbon dissociation.[[32,33] The more-graphitic carbon is formed by a catalytic process involving the surface diffusion of iron/iron hydrocarbon species across the edges of the layer planes of the deposited carbon. More iron atoms in the Fe-rich phases may diffuse to the layer planes in association with hydrocarbon species, and dissociation occurs at the edges of the layers, resulting in more-graphitic carbon formation.

Figure 4 shows a representative Raman spectroscopy mapping showing the spatial distribution and intensity of the phosphorous, iron, and D band, and the ratio of I_G/I_D measured in a selected area of the sample (the corresponding SEM and optical-microscopy image of the scanned area are also shown as the insets of Figure 4a and b, respectively). As shown in Figure 4c, the darkness in the phosphorous map indicates the deficiency

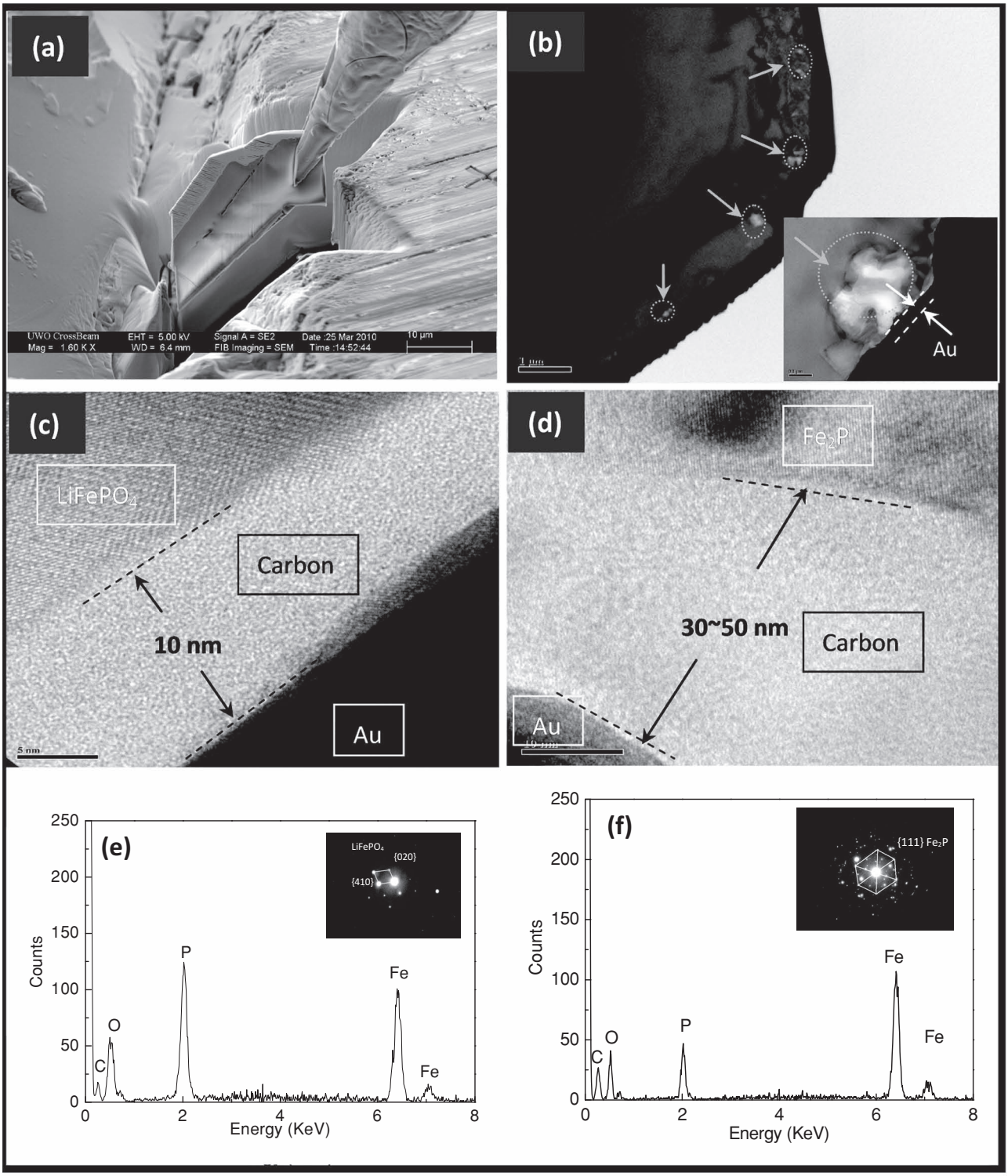

Figure 3. FIB and HR-TEM of carbon coating on Fe-rich impurities of $LiFePO_4$. a) The pickup process of the focused-ion-beam-etching sample. b) TEM images of Fe-rich impurities (marked by the arrows/dotted circles and enlarged in the inset figure) in the sample. c) HR-TEM of carbon coating on bulk $LiFePO_4$. d) High-resolution TEM of carbon coating on Fe-rich impurity phase. e) EDX of carbon coating on bulk $LiFePO_4$. f) EDX of carbon coating on Fe-rich impurity phase.

of phosphorous in this area. Similarly, iron was found to be enriched at the boundaries of this zone, as shown in Figure 4d, and more carbon was also coated on the same boundaries. Clearly, Fe-rich phases at these boundaries can catalyze the decomposition and deposition of the carbon precursor, contributing to more carbon coating. Moreover, from the Raman

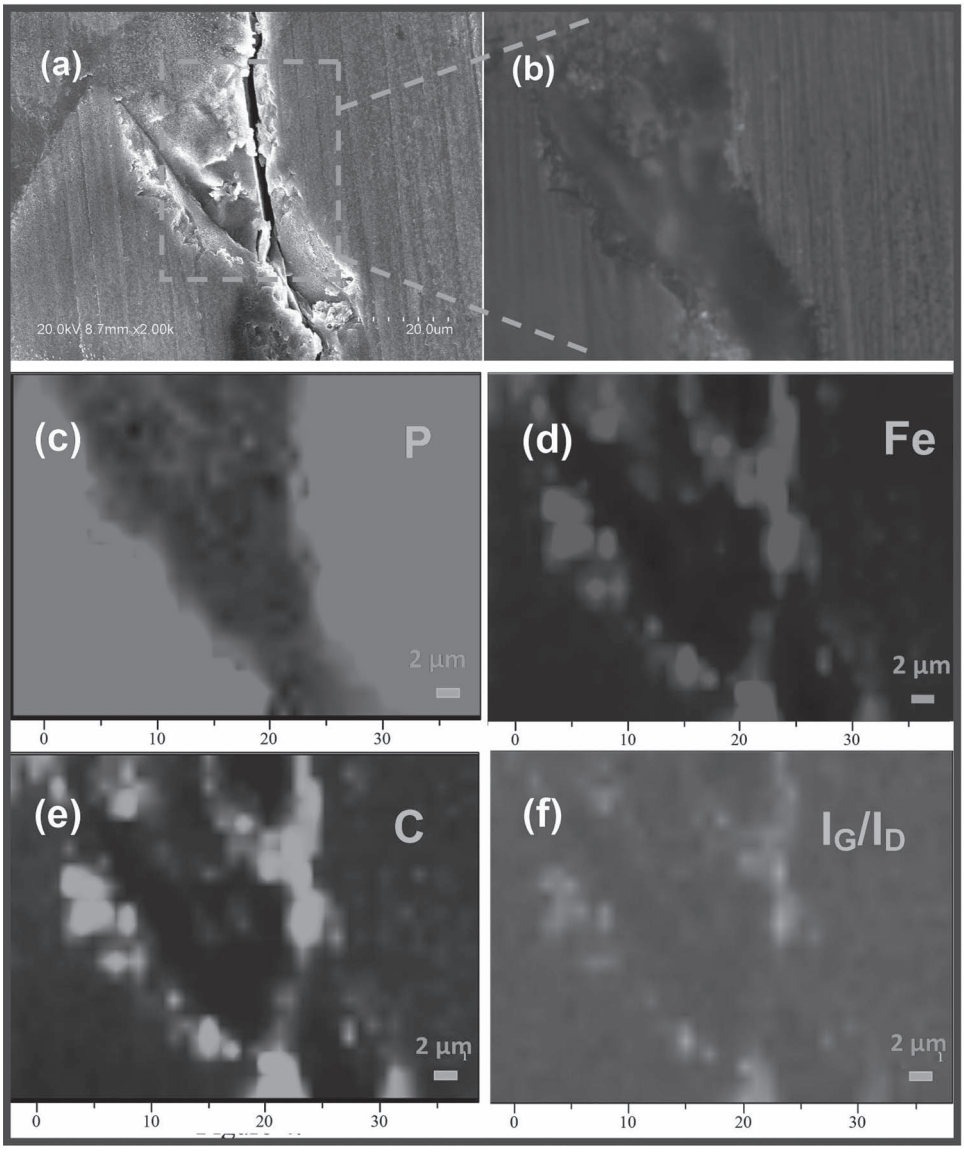

Figure 4. Raman spectroscopy mappings of carbon coating on the Fe-rich phases of $LiFePO_4$. a) SEM image of the Fe-rich phase. b) Optical image from micro-Raman spectroscopy at the Fe-rich phase. c–f) Raman spectroscopy mappings for phosphorus (c), iron (d), carbon (e), and the I_G/I_D of carbon (f).

spectroscopy mapping, a high I_G/I_D ratio was observed at the boundaries. These results suggest that the existence of Fe-rich phases not only results in the higher carbon content, but also contributes to the presence of more-graphitic carbon due to the graphitizing catalytic effect of the Fe-rich phases in the carbon formation. It is clear that the high amount of graphite in the formed carbon is more desirable in view of its contribution to the electronic conductivity (the electrical conductivity of graphite and acetylene black are 6.4×10^{-2} and 5.7×10^{-4} S cm^{-1} respectively).[34]

SEM images and representative Raman spectroscopy surface mappings obtained from a P-rich area are shown in **Figure 5**. The back-scattered-electron image in Figure 5b clearly shows the shape of the P-rich zone. The Raman spectroscopy mappings obtained from the dashed square zone are shown in Figure 5c–f. Obviously, this area is phosphorous-rich and iron-deficient, and less carbon was deposited on this phase. Moreover, this zone also gives less-graphitic carbon, as the low I_G/I_D ratio shown in Figure 5f. This Raman spectroscopy result suggests that the P-rich phase has a negative effect on the carbon coating by restricting carbon deposition and decreasing the graphitic carbon formation.

Figure 6 shows a schematic representation of the effect of impurity phases on the carbon coating on $LiFePO_4$. Fe-rich phases have positive effects on the decomposition/deposition of carbon precursors, contributing to thicker carbon films. On the contrary, carbon formation is inhibited at the P-rich phases, resulting in thin carbon coating and low carbon quality. This

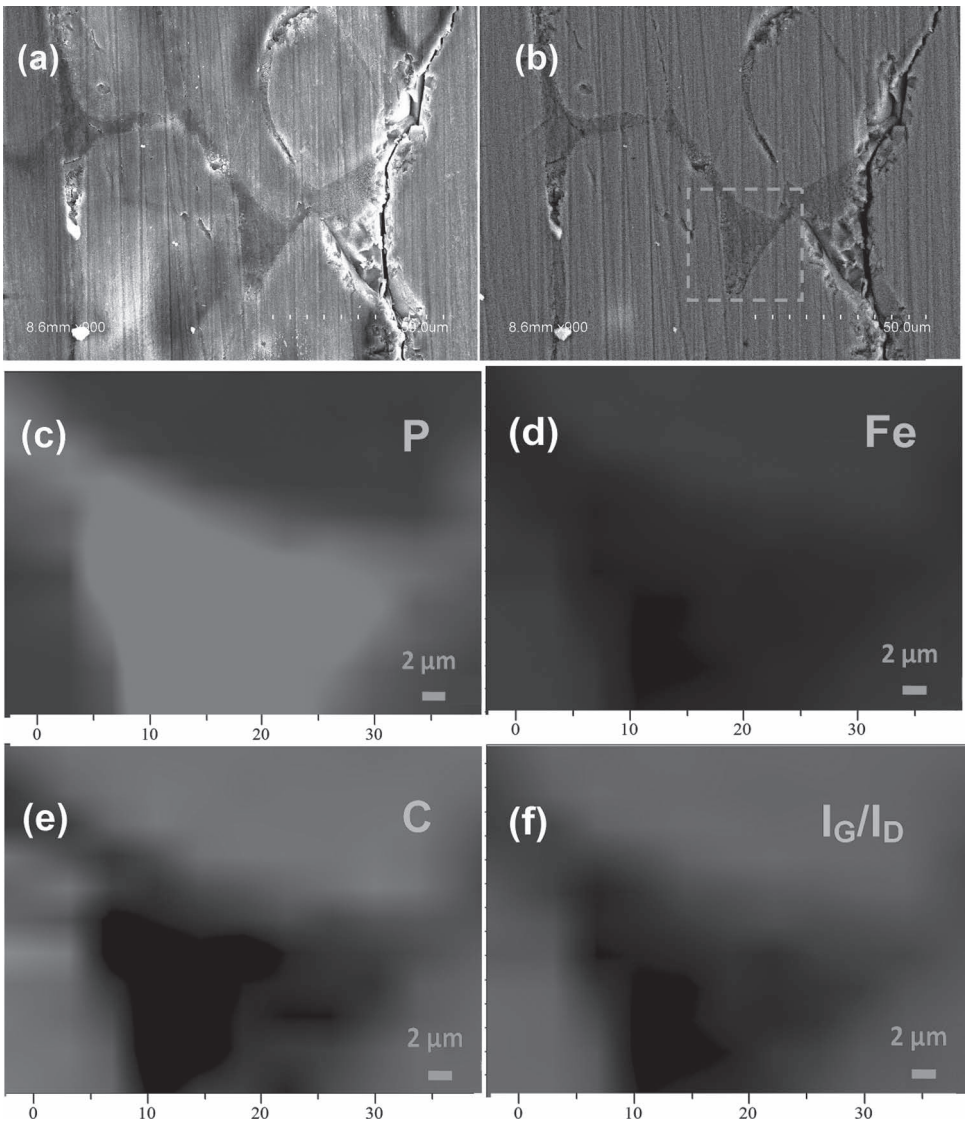

Figure 5. Raman spectroscopy mappings of carbon coating on P-rich phases of $LiFePO_4$. a) SEM image of the P-rich phase. b) Back-scattered electron (BSE) mode of the P-rich phase. c–f) Raman spectroscopy mappings for phosphorus (c), iron (d), carbon (e), and the I_G/I_D of carbon (f).

phenomenon can be attributed to the different catalysis properties of Fe- and P-rich phases during the carbon precursor decomposition/deposition process.

To confirm further the influence of impurities in $LiFePO_4$ on carbon coating and the generality of this phenomenon for common $LiFePO_4$ materials, commercial nano-$LiFePO_4$ powder (90 wt%) was mixed with some standard impurity (Fe_2P or $Li_4P_2O_7$) powders (10 wt%) before carbon coating. Figure S5 in the Supporting Information shows the XRD patterns of the three powder-based samples, and the added impurities were identified clearly. After carbon coating, obviously different carbon amounts were obtained for the three samples. As shown in the EDX analysis (Supporting Information, Figure S5b–d), the sample with added Fe_2P shows the highest carbon amount (30.5 at%), while $Li_4P_2O_7$ shows the lowest (18.3 at%). Considering that EDX is just semi-quantitative, TGA was also employed to determine the exact carbon content in the three samples (Supporting Information, Figure S6a). The carbon contents of pure $LiFePO_4$, Fe_2P added, and $Li_4P_2O_7$-added $LiFePO_4$ are 4.9 wt% (5.0 wt% – 0.1 wt%), 6.8 wt% (5.0 wt% + 1.8 wt%), and 3.8 wt% (5.0 wt% – 1.2 wt%), respectively, considering a weight gain of ≈5.0 wt% during the oxidation of $LiFePO_4$ to $Li_3Fe_2(PO_4)_3$ if the impurities' effects are neglected. These TGA results are consistent with the above EDX results, indicating that the impurities have a remarkable influence on carbon coating. Furthermore, Raman spectra of the three powder samples are also shown in Figure S6b in the Supporting Information. The I_G/I_D ratios of pure $LiFePO_4$, Fe_2P-added and $Li_4P_2O_7$-added $LiFePO_4$ are 1.13, 1.25, and 0.93, respectively. The higher ratio of the I_G/I_D indicates the high graphitic carbon content, thus the Fe-rich Fe_2P impurity improves the carbon quality, while for P-rich sample, the reverse is true. These impurities effects are consistent with the conclusions made above on ingot samples.

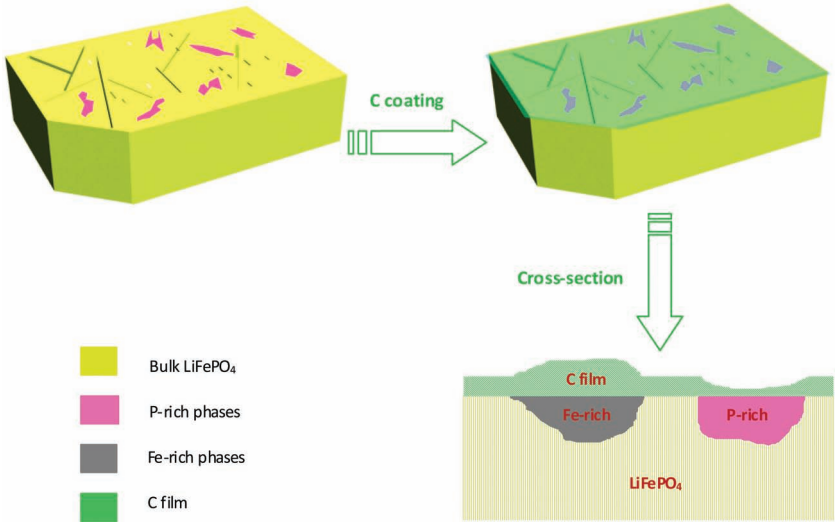

Figure 6. Schematic illustration of the carbon-film formation with different thickness on impurity phases at $LiFePO_4$ during carbon coating.

3. Conclusions

In this work, for the first time, we provide direct evidence regarding the significant effects of typical impurity phases in $LiFePO_4$ on the morphology and structure of a carbon coating on $LiFePO_4$. An ingot sample with a flat surface was used as a model material to allow us to observe, identify, and locate the impurity phases on its surface in comparison to carbon deposition on pristine $LiFePO_4$ crystal phases. SEM and micro-XRD identified the main impurity phases as P-rich and Fe-rich phases (mainly iron phosphide, Fe_2P). The presence of these two impurities has an important effect on carbon coating on $LiFePO_4$. The P-rich phase was found to have an inhibiting effect (or no positive catalytic effect) on carbon coating, compared with carbon on the $LiFePO_4$ bulk zone. In contrast, the Fe-rich phosphide (Fe_2P) shows a much higher carbon content where the carbon content is more than twice as much as that at bulk. Moreover, this Fe-rich Fe_2P could be responsible for the enhanced graphitic-carbon content in $LiFePO_4$. These findings provide an important guideline for the improvement of carbon-coating quality in C-$LiFePO_4$ composite materials. Furthermore, the methodology developed here will help us to understand and reveal the basic carbon-deposition process and structure on $LiFePO_4$, leading to the further-improved performance of this promising electrode material.

4. Experimental Section

Materials: The $LiFePO_4$ ingot sample was provided by Phostech Lithium Inc. (Montreal, Canada). The details of the melt-casting process can be found in previous work.[12] Here, to get a flat surface on the ingot sample, the melt sample was cut into a smaller size using a manual saw, and then the surface was polished using pieces of aluminum oxide sandpaper (London, 3M Canada) from coarse (Grit 120) to fine grades (Grit 1500). After ultrasonic cleaning in ethanol several times, a $LiFePO_4$ ingot sample with a clean and flat surface was thus obtained.

Carbon Coating: Carbon-coating experiments on ingot samples were performed in a spray-pyrolysis system, which was previously developed for the synthesis of various nanomaterials in our lab.[18–20] In the experiment, alcohol was used as the carbon precursor and argon acted as a carrying and protecting gas. Briefly, the ingot sample with the flat surface up was put in a quartz tube and Ar was introduced into the quartz tube for 20 min to eliminate the air. Subsequently the furnace was heated, and the carbon-coating process was performed at 650 °C for 20 min. After the carbon coating, the coated sample was cooled to room temperature within the furnace still under the protection of the Ar atmosphere. Carbon-coated $LiFePO_4$ (or with Fe_2P or $Li_4P_2O_7$ added) powder samples were prepared by the solid-state carbon-coating method. Lactose (carbon precursor) was firstly dissolved in either isopropyl alcohol or H_2O, and then the above $LiFePO_4$-based powder sample was added to the carbon-precursor solution. The suspension was mixed ultrasonically, and was then allowed to evaporate to dryness. The sample was further annealed at 700 °C for 1 h under Ar protection to form carbon-coated samples.

Characterization: The morphology and microstructure of the samples were characterized using an S-4800 scanning electron microscope (SEM) (Hitachi) equipped with an energy-dispersive X-ray microanalysis system and a field-emission gun. X-ray diffraction analyses of the ingot sample was performed using a Bruker D8-Advantage powder diffractometer with Cu K_α radiation (1.54056 Å) between 20° and 80° in reflection geometry. Focused-ion-beam lithography was used for in situ sectioning of the impurity phases, which were imaged and identified by SEM. The slicing process was performed on a LEO (Zeiss) 1540XB FIB/SEM (Western Nanofab., University of Western Ontario), and subsequently the slices were plucked using a nanomanipulator. After the tip of the end effector was folded over and removed from the nanomanipulator rod, the sample could be mounted in the HR-TEM sample holder. HR-TEM and EDX analysis at different phases were performed using a JEOL 2010 FEG instrument operating at an accelerating voltage of 200 kV. The diffraction patterns were also recorded using the selected area diffraction (SAED) mode. In order to determine the carbon nature at different phases on $LiFePO_4$, Raman spectra was recorded using a Raman spectrometer (HORIBA Scientific LabRAM HR) with a laser (λ = 532.4 nm) as the excitation source. Raman spectroscopy maps from different areas at the sample surface were collected in autofocus mode with a spatial resolution of ca. 0.7 µm. The average Raman spectra, as well as the average G-band to D-band intensity ratio (I_G/I_D) were calculated from all of the spectra in the Raman spectroscopy maps.

Supporting Information

Supporting Information is available from the Wiley Online Library or from the author.

Acknowledgements

This work was supported by the Natural Sciences and Engineering Research Council of Canada (NSERC), Phostech Lithium Inc., the Canada Research Chair (CRC) Program, the University of Western Ontario, and the MITACS Elevate Strategic Fellowship Program.

Received: May 15, 2012
Revised: July 4, 2012
Published online: October 1, 2012

[1] A. K. Padhi, K. S. Nanjundaswamy, J. B. Goodenough, *J. Electrochem. Soc.* **1997**, *144*, 1188–1194.
[2] N. Ravet, Y. Chouinard, J. F. Magnan, S. Besner, M. Gauthier, M. Armand, *J. Power Sources* **2001**, *97–98*, 503–507.
[3] J. Wang, X. Sun, *Energy Environ. Sci.* **2012**, *5*, 5163–5185.
[4] Z. R. Chang, H. J. Lv, H. W. Tang, H. J. Li, X. Z. Yuan, H. Wang, *Electrochim. Acta* **2009**, *54*, 4595–4599.
[5] Y. Hu, M. M. Doeff, R. Kostecki, R. Finones, *J. Electrochem. Soc.* **2004**, *151*, A1279–A1285.
[6] M. M. Doeff, J. D. Wilcox, R. Kostecki, G. Lau, *J. Power Sources* **2006**, *163*, 180–184.
[7] Y. Wang, Y. Wang, E. Hosono, K. Wang, H. Zhou, *Angew. Chem. Int. Ed.* **2008**, *47*, 7461–7465.
[8] X. L. Wu, L.Y. Jiang, F. F. Cao, Y. G. Guo, L. J. Wan, *Adv. Mater.* **2009**, *21*, 2710–2714.
[9] Y. H. Nien, J. R. Carey, J. S. Chen, *J. Power Sources* **2009**, *193*, 822–827.
[10] P. S. Herle, B. Ellis, N. Coombs, L. F. Nazar, *Nat. Mater.* **2004**, *3*, 147–152.
[11] Y.-H. Rho, L. F. Nazar, L. Perry, D. Ryan, *J. Electrochem. Soc.* **2007**, *154*, A283–289.
[12] M. Gauthier, C. Michot, N. Ravet, M. Duchesneau, J. Dufour, G. Liang, J. Wontcheu, L. Gauthier, D. D. MacNeil, *J. Electrochem. Soc.* **2010**, *157*, A453–462.
[13] S. Y. Chung, J. T. Bloking, Y. M. Chiang, *Nat. Mater.* **2002**, *1*, 123–128.
[14] B. Kang, G. Ceder, *Nature* **2009**, *458*, 190–193.
[15] K. Zaghib, P. Charest, M. Dontigny, A. Guerfi, M. Lagacé, A. Mauger, M. Kopec, C. M. Julien, *J. Power Sources* **2010**, *195*, 8280–8288.
[16] S. P. Ong, L. Wang, B. Kang, G. Ceder, *Chem. Mater.* **2008**, *20*, 1798–1807.
[17] M.-S. Song, D.-Y. Kim, Y.-M. Kang, Y.-I. Kim, J.-Y. Lee, H.-S. Kwon, *J. Power Sources* **2008**, *180*, 546–552.
[18] M. Ionescu, Y. Zhang, R. Li, X. Sun, *Appl. Surf. Sci.* **2011**, *257*, 6843–6849.
[19] J. Wang, Y. Chen, Y. Zhang, M. Ionescu, R. Li, X. Sun, S. Ye, S. Knights, *J. Mater. Chem.* **2011**, *21*, 18195–18198.
[20] J. Wang, G. Yin, Y. Chen, R. Li, X. Sun, *Int. J. Hydrogen Energy* **2009**, *19*, 8270–8275.
[21] F. Benissad-Aissani, H. Ait-Amar, M.-C. Schouler, P. Gadelle, *Carbon* **2004**, *42*, 2163–2168.
[22] E. Cruz-silva, D. A. Cullen, L. Gu, J. M. Romo-Herrera, E. Munoz-Sandoval, F. Lopez-Urias, B. G. Sumpter, V. Meunier, J. C. Charlier, D. J. Smith, H. Terrones, M. Terrones, *ACS Nano* **2008**, *2*, 441–448.
[23] M. W. P. Xu, J. J. Brown Jr., *J. Am. Ceram. Soc.* **1989**, *72*, 110–115.
[24] C. M. Burba, R. Frech, *J. Electrochem. Soc.* **2004**, *151*, A1032–A1038.
[25] M. Maccario, L. Croguennec, B. Desbat, M. Couzi, F. L. Cras, L. Servant, *J. Electrochem. Soc.* **2008**, *155*, A879–A886.
[26] R. Baddour-Hadjean, J. P. Pereira-Ramos, *Chem. Rev.* **2010**, *110*, 1278–1319.
[27] M. M. Doeff, Y. Hu, F. Mclarnon, R. Kostecki, *Electrochem. Solid-State Lett.* **2003**, *6*, A207–A209.
[28] X. Sun, R. Li, J. Dodelet, S. Désilets, *Carbon* **2007**, *45*, 732–737.
[29] A. Gohier, C. P. Ewels, T. M. Minea, M. A. Djouadi, *Carbon* **2008**, *46*, 1331–1338.
[30] T. Baird, J. R. Fryer, B. Grant, *Carbon* **1974**, *12*, 591–602.
[31] R. T. K. Baker, P. S. Harris, R. B. Thomas, R. J. Waite, *J. Catal.* **1973**, *30*, 86–95.
[32] H. P. Boehm, *Carbon* **1973**, *11*, 587–590.
[33] K. Hernadi, A. Fonseca, J. B. Nagy, D. Bernaerts, A. A. Lucasa, *Carbon* **1996**, *34*, 1249–1257.
[34] H. C. Shi, W. I. Cho, H. Jang, *Electrochim. Acta* **2006**, *52*, 1472–1476.